Anion polarization and the stability of layered structures in MX_2 systems

1994 J. Phys.: Condens. Matter 6 159

(http://iopscience.iop.org/0953-8984/6/1/017)

J. Phys.: Condens. Matter 6 (1994) 159–170. Printed in the UK

Anion polarization and the stability of layered structures in MX_2 systems

M Wilson and P A Madden

Physical Chemistry Laboratory, Oxford University, South Parks Road, Oxford OX1 3QZ, UK

Received 6 August 1993, in final form 21 October 1993

Abstract. The contribution of the induction energy to the stability of layered structures in MX_2 (halide) systems is investigated. A simple potential, based upon the ionic model but including many-body induced dipole effects in a self-consistent way, reproduces the experimental structure map for a wide range of materials. The predicted stability of the layered crystals is confirmed in molecular dynamics simulations at high temperatures. The potential role of other induction terms is briefly discussed.

1. Introduction

For the simplest model of an ionic system, in which the interactions are those of electronically rigid ions, crystal structures are predicted on the basis of radius-ratio rules (e.g. [1]). If these rules are applied to a selection of MX_2 systems, where M is a divalent metal and X a halogen, we find a pattern of the type indicated in figure 1. The cations and anions have been ordered according to their crystal radii [2] which are given in parentheses. The predicted trend is a reduction in coordination number with radius ratio: the critical ratios for a transition from one structure type to another are fluorite [8:4] 1–1.37, rutile [6:3] 1.37–2.44 and four-coordinated > 2.44. The radius ratio rules are partially successful with the MX_2 systems, as can be seen from a comparison of figure 1 with the 'structure-map' [1] in figure 2 based upon the ionic radii and the experimentally observed crystal structures. In particular, the transition from fluorite [8:4] to lower coordination rutile [6:3] and $PbCl_2$ [7+2] is successfully located. However, the radius ratio rules completely fail to account for the prevalence of layered structures in the top right-hand corner of the structure map. Because of this and since the layered structures involve adjacent layers of like-charged ions (in violation of the apparent need to minimize coulombic interactions) the systems which appear in this small-cation/large-anion corner are often regarded as partially 'covalent' [3].

The generic term 'covalency' covers a wide range of electronic phenomena. Barnes and Enderby [7] describe covalency broadly as 'interactions which change the charge distribution of the valence electrons ...'. To others (and most chemists), the term implies charge transfer. Since it is difficult to introduce *transferable* descriptions of the interactions in systems where charge transfer is significant without resorting to an explicit description of the valence electrons, it seems important to carefully examine the true limits of an ionic description. To this end we have recently been developing simulation models in which the full effects of electronic polarization are included within a basically ionic description—in the sense that the ions retain their formal charges and their properties are regarded as transferable from one system to another.

0953-8984/94/010159+12$07.50

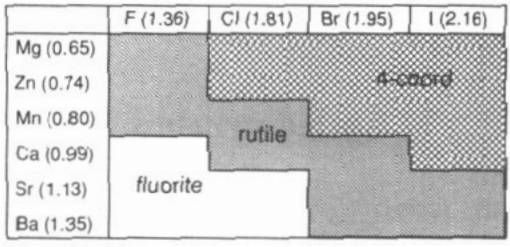

Figure 1. Structure map based on standard radius-ratio rules; the ionic radii are given in parentheses.

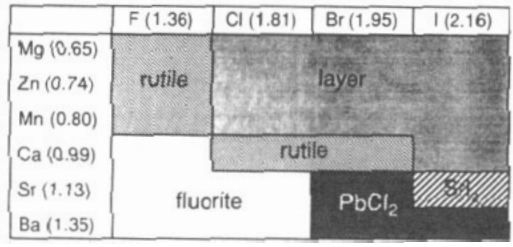

Figure 2. Experimental structure map.

A polarizable ion simulation model (PIM) has been described in detail in an earlier paper [4]. The method was inspired by Car and Parrinello's ideas [5] and Sprik and Klein's [6] way of treating polarization in a molecular system. The normal Born–Mayer interionic pair potential (the rigid-ion model, or RIM) is supplemented with a representation of the induced dipoles on the ions. The interaction between these polarized ions gives rise to the induction energy of the system. The non-additive, many-body aspects of the induction forces are included because the dipole on an ion is induced by the coulomb field arising from the charges and dipoles on the other ions, and is calculated in a self-consistent way. The short-range, overlap interactions which influence these dipoles ('induction damping terms') are also incorporated. The substantial difference from the shell model [8] is that the magnitude of the induced dipoles is governed by the true 'in-crystal' ion polarizability and the induction damping is not linked *a priori* to the Born–Mayer potential itself. The parameters which govern these terms are obtained, in principle, from electronic structure calculations. If the system crystallizes in a cubic crystal, the remaining parameters in the Born–Mayer potential may be obtained from crystal energetics [10] since in these cases the high symmetry of the crystal precludes induction interactions and the identification of the terms in the pair potential is unambiguous.

In a recent publication, we have shown how a stripped-down version of this model (in which dispersion and induction-damping terms are neglected and where the same Born–Mayer repulsion range parameter is used, irrespective of the cation identity) accounts for the experimentally observed structural trends in molten MCl_2 salts [9] as the cation radius is varied. In the present paper, we intend to show that a similar simplified model accounts for the crystal structures of a wider range of MX_2 systems, linking them simply to the cation radius and the anion polarizability. In including only the barest details in the potential, the intention is to highlight the role of polarization effects, *within an ionic model*. The crucial ideas are that ion polarization favours the lowering of the symmetry around the anionic site and that the resulting induced dipoles may efficiently screen the coulombic repulsion between the highly charged cations.

2. The model

2.1. Parameters of the model

In general, we include the short-range, overlap-repulsion and dispersion interactions between the ions by including a pair potential of Born–Mayer form; i.e.

$$u(r_{ij}) = A_{ij}e^{-a_{ij}(r_{ij}-(\sigma_+ + \sigma_-))} - \frac{C_{ij}}{r_{ij}^6} - \frac{D_{ij}}{r_{ij}^8} + \frac{Q_i Q_j}{r_{ij}} \qquad (1)$$

where the parameters A_{ij}, a_{ij}, C_{ij} and D_{ij} have their usual meaning [8]. In order to focus on the subtle structural effects which arise from the interplay of the induced dipoles on the anions and short-range forces we neglect any contributions to the potential which do not influence the structure. We choose the remaining parameters in the spirit of a strict ionic model, in which formal charges are used for Q_+ and Q_- and in which the anion properties are kept constant, irrespective of the particular cation. For a given anion, we will describe the results from a series of calculations with potentials which differ only in the choice of cation radius σ_+, for which we use the values in [2]. The anion radii are taken from standard tables [2]. The amplitude, A_{+-}, and range, a_{+-}, of the short-range repulsion between cations and anions are fixed at a constant value for all systems studied, the value of a_{+-} being 1.6 au and A_{+-} being 7.75×10^{-3} au from [8]. For the anion–anion interactions B_{--} and a_{--} were taken from standard sources [8] (where $B_{--} = A_{--}e^{a_{--}*\sigma_{--}}$), see table 1. The short-range cation–cation interaction is neglected; coulomb repulsion between these doubly charged species is sufficient to keep them beyond the range of overlap of their electron clouds. We include an anion–anion dipole dispersion term C_{--} but neglect the cation–cation and cation–anion dispersion interactions, which would be expected to be considerably smaller. In a detailed account of the crystal energetics we would expect to have to include these interactions, but as we shall show, they are not necessary to recover the observed structural trends. We omit C_{+-} and C_{++} and all the quadrupole dispersion terms because reliable values are not available from electronic structure calculations for a wide range of systems, so that to include them we would have to introduce a large number of ill-determined parameters into the model. For the three C_{--} parameters we base our values on the *ab initio* results of Pyper [10]: these are given in table 1.

Table 1. Short range, polarizabilities and dispersion parameters for the anions under investigation (all in atomic units).

Anion	a_{--}	B_{--}	α	C_{--}
Cl	1.67	128.24	20.0	200.0
Br	1.56	140.63	30.0	350.0
I	1.37	113.83	45.0	600.0

Induction terms are incorporated as described in our earlier paper [4]. Note that adding induction effects to the Born–Mayer potentials is not inconsistent as the pair induction terms, which would be proportional to r_{ij}^{-4}, are explicitly *excluded* from the Born–Mayer form since in cubic crystals the pair charge-induced dipole is completely cancelled by a three-body term due to the high symmetry. In crystals of lower symmetry these terms survive and, as we will show, play an important role. In specifying the terms responsible for the induction effects we neglect the role of induced dipoles on the cations; we can anticipate that these will be much less important than those on the anions. The induction energy of the cation charge with the anion polarizability is proportional to $Q_+^2\alpha_-$, compared with $Q_-^2\alpha_+$ for the anion charge with the cation polarizability. Even the most polarizable cation Ba^{2+}, in $BaCl_2$, $Q_+^2\alpha_-$ is larger than $Q_-^2\alpha_+$ by a factor of 8. The induction effects are therefore specified by the anion polarizability for which we take the in-crystal value (table 1) as given in reference [10, 11] for each anion series: in reality, of course, some variation with cation is expected [10, 12]. In, addition we need to specify the short-range, induction-damping terms. We have shown previously how these effects can be introduced into the simulation model in a self-consistent way such that the effective induction damping

between an isolated ion pair has the Tang–Toennies form [13]

$$f(r_{ij}) = 1 - e^{-b_{ij}r_{ij}} \sum_{k=0}^{4} \frac{(b_{ij}r_{ij})^k}{k!} \tag{2}$$

which requires the specification of a parameter b_{ij}, which controls the range of the induction damping for each pair of ions. To avoid a proliferation of parameters, we tie this range to the Fumi–Tosi ion radii by setting

$$b = c(\sigma_+ + \sigma_-)^{-1}. \tag{3}$$

In order to generate all the crystal energies quoted below, we used only a single value for the parameter c, which sets the scale of the induction damping on the sum of ionic radii. The crystal energies are quite sensitive to the value used for this parameter. We chose a value of 4.65 which is close to the result we obtained by fitting the *ab initio* data for distortion-induced dipoles in LiF [12] to the Tang–Toennies functional form [13].

In summary, we have set up a general potential model which includes the minimum number of parameters. Except for the ionic radii, for which literature values are used, we employ only 11 parameters for all the chlorides, bromides and iodides in table 1. These parameters take physically reasonable values which can be supported from independent sources. They are held constant for each ion over the full range of systems included in our study.

We have carried out calculations of two types with this model. Firstly, we have calculated the energies of the crystal structure at 0 K in order to show how the lowest energy crystal structure is influenced by the cation radius in the presence of induction effects. Secondly, we have run molecular dynamics computer simulations at reasonably high temperature (but below the experimental melting temperatures) in order to demonstrate that the crystal structures we find from the simple energetic calculations are truly stable.

3. Perfect crystal energetics

3.1. Calculating the crystal energies

For the potential parameter sets associated with each of the systems appearing in table 1, we have calculated the minimum energy in four basic crystal structures: fluorite, $PbCl_2$, rutile and $CdCl_2$. These may be taken to exemplify the different coordination combinations [8:4], [7+2], [6:3] and layered. In reality more crystal types than these are found in the systems included in our structure map; however, the more unusual types are closely related to one of these four and may be considered to belong to the same structure class for our purpose of eliciting structural trends. For example, the layered systems may crystallize in either $CdCl_2$ or CdI_2 which differ only in the stacking of the hexagonal layers. Further, SrI_2 forms a unique structure, but it is very similar to $PbCl_2$ in its coordination and we may expect it to give a similar energy. Recently [15] it has been shown that $ZnCl_2$ crystallizes into a layered structure with the Zn ions in tetrahedral sites (as opposed to distorted octahedra in $CdCl_2$ or CdI_2); we will return to this distinction in the discussion.

We first calculate the lattice parameter R_0 which minimizes the energy with the ions placed in appropriate positions for each crystal structure. In order to do this we 'anneal' the values of the induced dipoles (as described in [4]) until they reach their self-consistent values at several values for the lattice parameter and determine the total energy. We then fit

these energies to a parabola to locate R_0 and the crystal energy. For the layered structure we used idealized ion positions in which the anions are in a perfect FCC lattice and the cations occupy alternate layers of octahedral holes. For the other structures we have used the literature [14] values for the ionic positions, where available; otherwise, for the rutile structure we used the ion positions within the unit cell for $CaCl_2$ [14] and for the $PbCl_2$ structure we used the ion positions for this compound. In the case of the fluorite structure the anions are in a symmetric environment and so the electric field at the anion site is zero leading to no induced dipoles. In this case a static rigid ion (RIM) calculation will suffice. The quoted energies are the crystal energies at R_0.

3.2. Results

Figure 3 shows the crystal energy versus the cation radii for the dichlorides. As the cation radius increases we see that the energetically favourable structure changes in the order layered ⟶ rutile ⟶ fluorite. Comparison with the structure map of figure 2 (looking down column 2) shows that this is the experimentally observed *trend*. We would not expect the phase boundaries to be located exactly with our simple model, as many deatils of the interionic interactions are neglected or simplified. For example, inclusion of cation–anion dispersion terms ($C_{+-} \neq 0$) would (slightly) stabilize the structures with high coordination numbers.

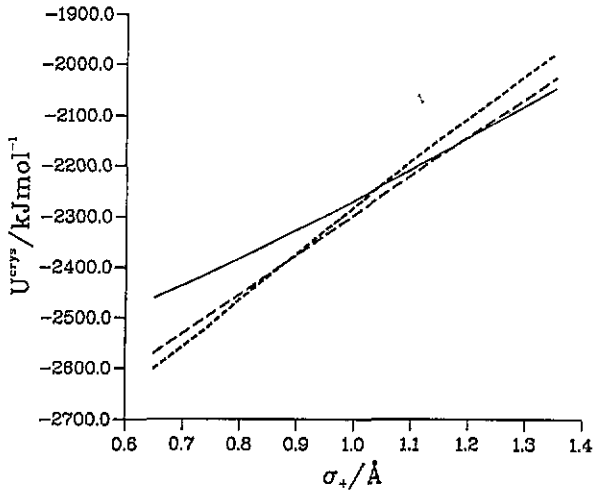

Figure 3. The MCl_2 crystal energies for the PIM are plotted versus the cation radius. The full line is for the fluorite structure, long-dashed for rutile and short-dashed for layered. The figure indicates a transition from fluorite to rutile between Sr and Ca, and from rutile to layered between Ca and Mn, in agreement with figure 2.

The crystal energies for the dibromides are shown in figure 4. Again, the observed trend of layer ⟶ rutile ⟶ $PbCl_2$ is consistent with the structure map. It is worth noting that the figure implies that, if a large enough cation could be found, then the fluorite structure could be energetically favourable. This seems intuitively reasonable as there are many fluorite fluorides but only a few chlorides with the fluorite structure. As the anion radius increases, six fold coordination around the cation becomes favoured over eight.

Figure 5 shows the crystal energies for the diiodides. Again, the observed trend of layer ⟶ $PbCl_2$ is consistent with the structure map. As can be anticipated from the dibromide

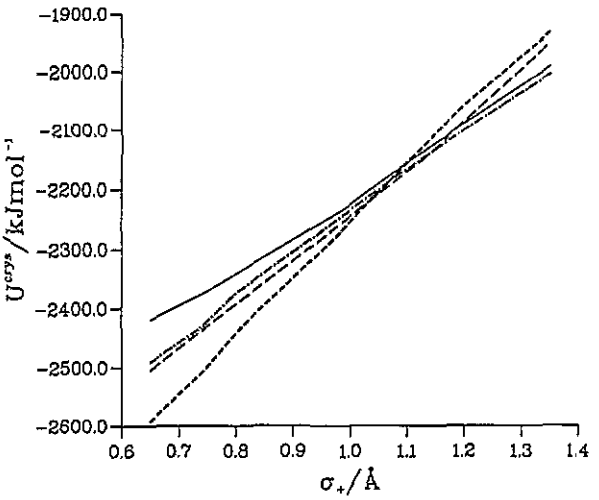

Figure 4. The MBr_2 crystal energies for the PIM. The symbols are as in figure 3, with the addition of $PbCl_2$, dashed-dot. Note the agreement with figure 2.

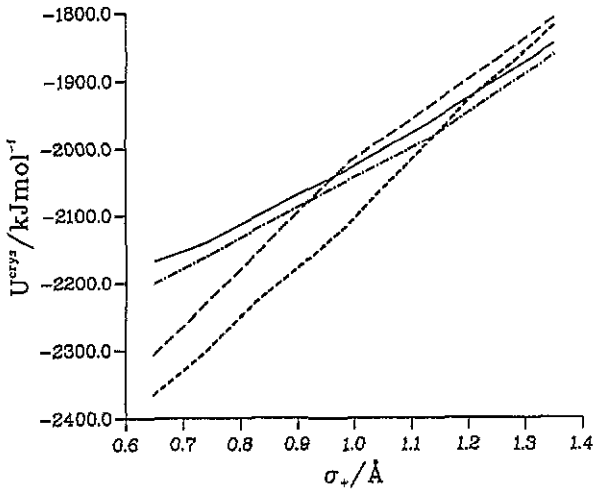

Figure 5. The MI_2 crystal energies for the PIM. The symbols are as in figure 4. Note the agreement with figure 2.

discussion above, for the diiodides the fluorite structure is much less stable than the other structures within the range of cation radii covered in our survey.

3.3. Discussion: the importance of anion polarization

The data discussed above shows that with the simple potential and varying only the cation radius we can recover the experimental structure map (figure 2) and, in particular, account for the appearance of layered structures in the top right-hand corner of the map. We can rationalize the observed trends by considering each of the four structure types in turn.

In the fluorite lattice (*Fm3m*) the cations are in an FCC arrangement with the anions occupying all the tetrahedral holes [14]. The cations are surrounded by eight nearest

neighbour anions. If we assign r_{AA} as being the closest anion–anion distance then r_{CC}, the nearest cation–cation distance, is $\sqrt{2}r_{AA}$. Thus, the singly charged anions are closer together than the doubly charged cations, a favourable arrangement for minimizing the total coulomb interaction of the formal charges. Note that the electric field at each anion site is zero, due to the tetrahedral symmetry, so that there are no induced dipoles in this structure.

In the rutile structure (*P4/mnm*) the anions are in a distorted close-packed environment with cations in the near octahedral holes [14]. The cations are surrounded by six nearest neighbour anions, hence this structure becomes favoured over fluorite on radius ratio considerations. In addition, the anions are sitting in an asymmetric site where the electric field due to the formal charges on the other ions may be non-zero and may cause induced dipoles. The dipoles lie in the a_0, b_0 plane.

The $PbCl_2$ (*Pbmn*) is the most complicated of the four main structural types, having twelve ions in the unit cell [14] each cation is surrounded by seven anions at a distance between 2.85 and 3.08 au in $PbCl_2$ itself. The anions sit in two distinct environments, both of which are asymmetric and can support induced dipoles.

In the layered structures the anions are close-packed, either hexagonal (CdI_2;$C\bar{3}m$) or cubic ($CdCl_2$;$R\bar{3}m$). *Alternate* layers of octahedral holes are filled by cations, thus the cations have six nearest neighbour anions. Note that $r_{CC} = r_{AA}$ in this structure, hence, based purely on a RIM, the layer structure will be disfavoured with respect to the fluorite, rutile or $PbCl_2$ because of the close approach of the doubly charged cations. However, the induction effects may be pronounced in this structure. Figure 6 shows a portion of the layered structure (CdI_2). We see that the anions are asymmetrically coordinated by cations, because only alternate layers of octahedral holes are occupied. Consequently, large dipoles are induced on the anions, the positive and negative poles of these dipoles are indicated by the shading of the anions. It can be seen that the dipoles stabilize a single X–M–X 'sandwich' of the layered structure by *screening* the repulsion between adjacent cations (the direction of the dipoles is such as to place negative charge in between the cations). It is for this reason that the cation–cation and anion–anion separations become equal in the layered structure. This discussion is reminiscent of our account [9] of screening in MX_2 melts and of the consequent prevalence of bent M–X–M bridge structures in these systems. Besides stablizing an X–M–X sandwich, the induced dipoles also contribute to an attractive interaction between adjacent anion sheets and help to balance the direct coulomb repulsion of the anion charges. It is clear from figure 6 that the *inter*sheet anion charge–dipole interaction is favourable; what is less clear is that the *inter*sheet dipole–dipole interaction is not pushing the sheets apart as might be anticipated from the direction of the dipoles. A dipole in one layer points into a triangular hole between the anions in the adjacent layer; in this alignment the intersheet dipole–dipole force becomes attractive for small intersheet separations. For a perfectly close-packed anion sublattice the four atoms form a tetrahedron, and the force is close to zero. Overall, although the layered structure is destabilized by the cation–cation and *in-plane* dipole–dipole interactions it is *stabilized* by the charge–dipole and *inter*sheet dipole-interactions so that for large anion polarizability and small cations it becomes the favoured structure. Besides the effects discussed above, the binding between the sandwiches has an important contribution from dispersion interactions, as recently demonstrated in a set of *ab initio* calculations [16, 17].

To illustrate the balance of these effects we show in figure 7 the variation in crystal energies for the dibromides predicted on the basis of a simple RIM, i.e. simply the energy of the pair potential terms and neglecting all induction effects. Comparison with figure 4 gives an idea of the importance of the induction energy. The layered system is unstable with

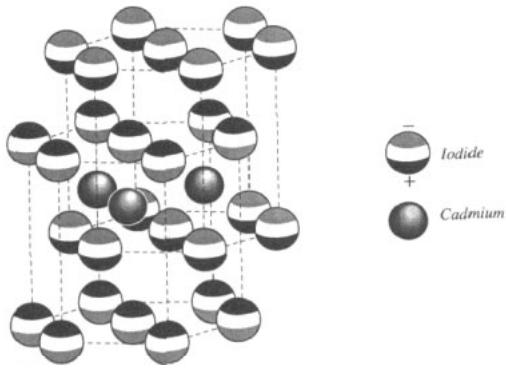

Figure 6. A schematic diagram of the layered structure (CdI_2) with the charge reorganization associated with the induced dipoles indicated by the shading of the anions.

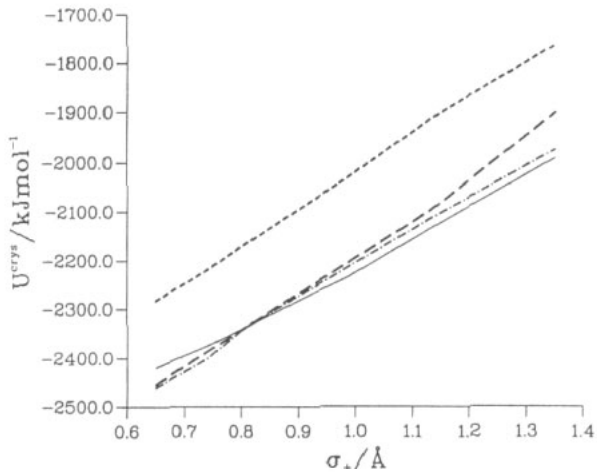

Figure 7. The MBr_2 crystal energies from the RIM are shown for comparison with the PIM data of figure 4, to emphasize the role of the induction energy. The symbols are as in figure 4.

respect to the fluorite across the whole range of cation radii. The rutile and $PbCl_2$ structure are also destabilized by omission of the induction term, but to a much lesser extent.

We have also referred to the sensitivity of the results to the short induction damping. In order to demonstrate this we show in figure 8 the effect of neglecting the induction damping altogether in calculations on the dibromides at the optimum lattice parameters determined for the full model (i.e. as in figure 4). Since now the dipoles induced by a given electric field are much larger than when induction damping is included, we see that the role of the polarization energy becomes still more pronounced (to the point at which the predicted most stable structures disagree with the experimental structure map of figure 2).

For the layered structure, the induction energy is a large fraction of the energetic terms incorporated in the RIM. For $MgBr_2$ the induction energy is 12.5% of the Madelung and dispersion energies in the full model, including induction damping, and would be a considerably larger fraction if induction damping were neglected.

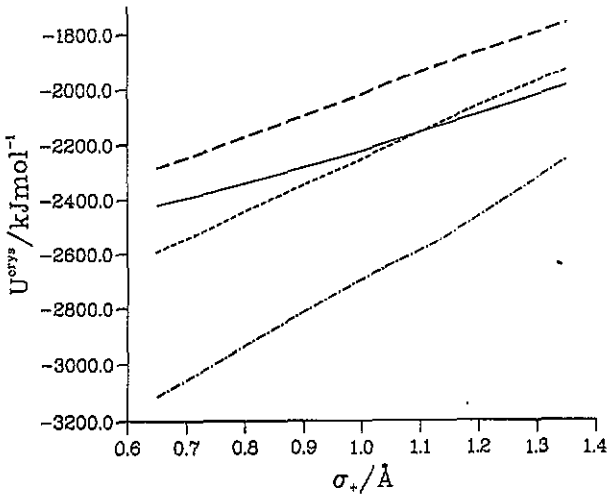

Figure 8. The effect of varying the range of the induction damping is illustrated for the MBr_2 crystal energies in the layered structure. The long-dashed line is the RIM, short-dashed is the PIM, dashed-dot is with no induction-damping: the energy of the fluorite structure is shown for comparison, full line.

4. MD simulations

We have carried out MD simulations on the layered structure in order to test the stability at elevated temperatures of the crystal structures predicted on the purely energetic criterion. The simulations are NVT on 384 ions (corresponding to 8 unit cells) and the potential parameters are those appropriate to $MgCl_2$. The temperature of the simulation is 1200 K. To monitor the crystal stability we have used the 'neutron' scattering structure factor from the cations at the $(2\pi/L)(2, 2, 2)$ wavevector, where L is the equilibrium simulation cell size. This corresponds to the Bragg vector associated with the scattering from successive layers of cations and is thus a good indicator of the layered structure. Figure 9 shows a comparison of the structure factors obtained from the polarizable and rigid models. The figure demonstrates the stability of the layered structure in the PIM (at least on this short timescale) whereas the layered structure collapses rapidly in the RIM. In figure 10 we show a molecular graphics snapshot [18], of the ionic positions in the course of the PIM run, which shows more directly that the layered structure is preserved with the ions performing small amplitude oscillations about their equilibrium positions.

Other simulations show that the layered structure is stable over indefinitely long runs. We have performed similar MD calculations on the fluorite and rutile structures with the PIM and again confirmed their stability in their predicted ranges.

5. General discussion: the importance of other effects

We have shown how inclusion of induced anion dipole interactions in a simple ionic model leads to a stabilization of layered structures for large values of the anion/cation radius ratio. The calculations account for the experimental structure map for a range of halides: note too that the same model has worked well for the corresponding melts [9].

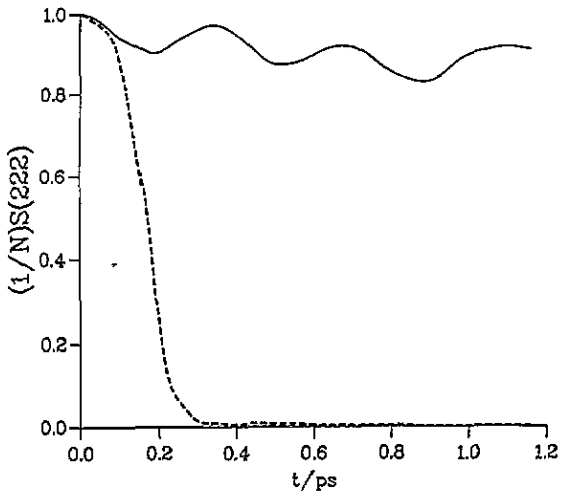

Figure 9. The normalized (2,2,2) structure factor for the cations in PIM (full line) and RIM (dashed) simulations of $MgCl_2$.

In fact, our selection of systems has been rather conservative. The structural trends in a large number of divalent transition and post transition metal halides can also be accounted for by the simple model we have described. With the exception of Mn^{2+}, which has a spherical d^5 electronic configuration, we have excluded the transition metals from the survey because they raise the spectre of specific electronic effects. Post transition metals may require the inclusion of extra polarization effects to be accurately described. Figure 11 shows a tentative extended structure map based on the same principles as figure 2, i.e. the normally quoted ionic radii. The only exception is that the order of Pb and Sr is reversed for reasons we discuss below (i.e. we treat Pb as smaller than Sr, whereas the crystal radius is larger). With regard to figure 11 we note that the layered structures are the dominant structural form in the divalent metal halides (in fact there are 29 on this map out of 45 possible compounds, excluding the fluorides). We see also that the general trends of figure 2 are preserved but with some interesting additions. For the two cations even smaller than Mg^{2+} (radii: Pd, 0.50 Å; Pt, 0.52 Å[2]) we see the emergence of chain-like structures not encountered on our previous structure map. Our feeling is that these structures still fit into the ionic model but represent polarization effects even more extreme than in the layer compounds.

Although our model works well in broadly accounting for the transition to layered structures, we believe that quantitative prediction of the properties of specific systems would be improved by including additional polarization effects within the basic ionic model. Amongst these additional effects we would list: cation polarization; higher order induced multipoles; and the change in anion properties with the size and coordination number of the cation.

It does not appear that *dipole* polarization of the cations plays a significant role in determining equilibrium structures (though it is important in crystal dynamics). The reasons for this are that cation polarizabilities are smaller than anion ones and, more generally, because the cations are located in symmetrical sites, where induced dipoles cannot form. Note, however that we have also neglected cation *dispersion* interactions; these may become significant for the more polarizable cations (see below).

Higher-order polarization of the cations may be a very significant effect and may be a major cause of cation specific effects, such as the fact that the Zn^{2+} ion prefers a tetrahedral

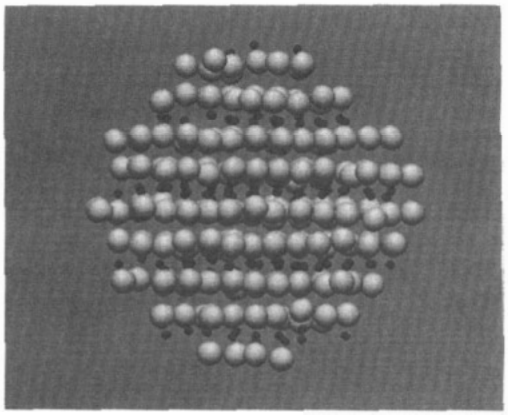

Figure 10. A snapshot of the ionic positions in the PIM $MgCl_2$ simulation at 1200 K.

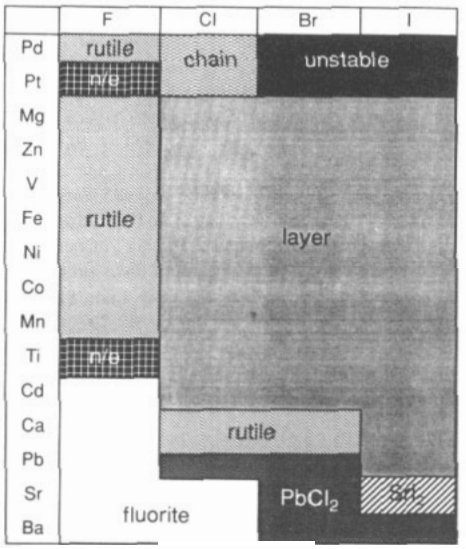

Figure 11. A structure map for an extended range of metal halide systems, indicating the preponderence of layered structures. n/e indicates that no data could be found for these entries; unstable means that the elements do not form 3D structures with these stoichiometries.

site in a layered structure, whereas the smaller Mg^{2+} ion is 6-fold coordinated. Mahan [19] has argued that, for the post-transition elements, the *octupole* polarizability may be particularly large and that this polarizability can lower the energy of a Zn^{2+} in a tetrahedral site but not an octahedral one. Similarly we find that Pb^{2+} fits perfectly into the extended halide structure map (figure 11) if it is assigned a smaller crystal radius than Sr^{2+}. This may indicate the operation of some other cation–anion attraction in PbX_2 which is insignificant in SrX_2, which could be the higher-order induced multipole or the neglected dispersion term (Pb^{2+} is appreciably more polarizable than Sr^{2+}). The recent *ab initio* electronic structure calculations of Harrison *et al* [16, 17] on $MgCl_2$ point to a role for higher-order induced multipoles on the *anions*. It is clear from figure 4 of [16] that the distortion of the Cl^- by the surrounding cations is not simply dipolar in nature.

In order to make further progress to clarify the influence of these additional effects, information on the relevant polarizabilities and the dependence of anion properties on the identity of the cation is required from electronic structure calculations. It should be clear that the methodology we have outlined can readily be extended to incorporate these effects so that simulations can be used to make a link between the electronic structure calculations and the properties of materials. In this way we would hope to establish the true limits of the ionic model.

References

[1] Müller U 1991 *Inorganic Structures* 2nd edn (New York: Wiley)
[2] Stark J G and Wallace H G 1984 *Chemistry Data Book* 2nd edn (London: John Murray)
[3] Rovere M and Tosi M P 1986 *Rep. Prog. Phys.* **49** 1001

[4] Wilson M and Madden P A 1993 *J. Phys.: Condens. Matter* **5** 2687
[5] Car R and Parrinello M 1985 *Phys. Rev. Lett* **55** 2471
[6] Sprik M and Klein M L 1988 *J. Chem. Phys* **89** 7556–66
[7] Enderby J E and Barnes A C 1990 *Rep. Prog. Phys* **53** 85
[8] Sangster M J L and Dixon M 1976 *Adv. Phys* **23** 247–342
[9] Wilson M and Madden P A 1993 *J. Phys.: Condens. Matter* **5** 6833
[10] Pyper N C 1991 *Adv. Solid State Chem.* **2** 223
[11] Fowler P W and Madden P A 1985 *Phys. Rev.* B **31** 5443
[12] Fowler P W and Madden P A 1984 *Phys. Rev.* B **29** 1035,
[13] Tang K T and Toennies J P 1984 *J. Chem. Phys.* **80** 3726
[14] Wyckoff R W G 1965 *Crystal Structures* (New York: Interscience)
[15] Desa J A E, Wright A C, Wong J and Sinclair R N 1982 *J. Non-Cryst. Solids* **51** 57
[16] Harrison N M and Saunders V R 1992 *J. Phys.: Condens. Matter* **4** 3873
[17] Harrison N M, Saunders V R, Aprà E, Causà M and Dovesi R 1992 *J. Phys.: Condens. Matter* **4** L261
[18] Advanced Visualisation Software Ltd, licensed through the University CHEST scheme
[19] Mahan G D 1980 *Chem. Phys. Lett.* **76** 183